Problem hardness of diluted Ising models: Population Annealing vs Simulated Annealing

Fernando Martínez-García[1] and Diego Porras[1]

[1]*Instituto de Física Fundamental IFF-CSIC, Calle Serrano 113b, Madrid 28006, Spain*

Population annealing is a variant of the simulated annealing algorithm that improves the quality of the thermalization process in systems with rough free-energy landscapes by introducing a resampling process. We consider the diluted Sherrington-Kirkpatrick Ising model using population annealing to study its efficiency in finding solutions to combinatorial optimization problems. From this study, we find an easy-hard-easy transition in the model hardness as the problem instances become more diluted, and associate this behaviour to the clusterization and connectivity of the underlying Erdős-Rényi graphs. We calculate the efficiency of obtaining minimum energy configurations and find that population annealing outperforms simulated annealing for the cases close to this hardness peak while reaching similar efficiencies in the easy limits. Finally, it is known that population annealing can be used to define an adaptive inverse temperature annealing schedule. We compare this adaptive method to a linear schedule and find that the adaptive method achieves improved efficiencies while being robust against final temperature miscalibrations.

I. INTRODUCTION

The field of combinatorial optimization aims to find a solution that minimizes an objective function from a set of finite candidate solutions. Although this set of potential solutions is finite, it is often so large that searching for the optimal solution through brute force is not practical. Many tasks of interest can be framed as combinatorial optimization problems, making this field of research highly relevant in industry - with examples such as logistics [1, 2] and finance [3–5] - and science, with one of the most important cases being statistical physics. The study of statistical physics models, such as the Ising Hamiltonian, is usually associated with simulating their low-temperature phases and finding the ground state configurations and corresponding energies, where some of the most challenging models are those describing spin-glasses [6, 7]. However, studying the ground states of three and higher-dimensional Ising spin glasses is known to be an NP-hard combinatorial optimization problem [8, 9].

Due to the difficulty and importance of finding solutions to complex statistical physics models, creating and improving algorithms for finding ground states has been the subject of considerable effort. The most popular approach is based on Monte Carlo algorithms, such as simulated annealing [10], parallel tempering [11], or population annealing [12, 13] to produce approximate samples from the Boltzmann distribution. These methods have demonstrated their utility for finding ground states and studying the thermal properties of these systems. Furthermore, Monte Carlo methods have proved very useful in providing heuristics for combinatorial problems beyond the field of statistical physics [1, 4, 5, 10]. However, the application of these methods to general combinatorial optimization problems faces significant differences with respect to the problems for which they were originally developed. General optimization problems in logistics or finance typically lack the regular connectivities between variables that are found in spin-lattice models. Further-

more, objective functions can take complex mathematical forms that complicate estimating typical energy scales and choosing hyperparameters such as annealing temperatures [14]. Population annealing is an auspicious approach to addressing these limitations. As we explain in more detail below, this algorithm provides us with an improved method for sampling Boltzmann distributions, together with an adaptive temperature schedule that facilitates its application to a diverse range of objective functions. Given the potential of population annealing for combinatorial optimization, it is relevant to gain insights into what advantages it offers depending on the characteristics of the targeted optimization problems.

The Population Annealing (PA) algorithm is a modified version of Simulated Annealing (SA). Both algorithms attempt to generate samples distributed according to a target thermal distribution at a given temperature. This is done by following the Metropolis-Hastings rule [15] at intermediate temperatures following an annealing temperature schedule that slowly brings the system to the target temperature. However, the PA algorithm differs from SA by introducing a resampling step between samples (also called *replicas*) at each temperature step. This step helps the system to stay closer to the correct thermal distribution by relocating samples that would otherwise be trapped at a local minimum. The effect of this additional step has been studied for spin-glasses in a 3D Edwards-Anderson model with Gaussian disorder [16] and demonstrated an improved efficiency of PA over SA for finding ground states for this family of problems, and a similar efficiency as parallel tempering. However, these results can be complemented by studying the problem hardness and the relative efficiency improvement of PA over SA for other problem families.

In this work, we study the relative behaviour of PA compared to SA when finding ground state configurations of random graphs. The study of random graphs is related to a variety of real-world problems, with examples such as internet topology [17, 18], social networks [19, 20],

and spread of diseases through populations [21]. In this work, we consider the case of the diluted Sherrington-Kirkpatrick Ising model [22] and study the relative efficiency between the SA and PA algorithms as a function of the connectivity of the models under consideration (parameterized by a value p), from sparse graphs up to all-to-all graphs. By considering this family of problems and using PA to obtain the values of the *entropic family size* [23] and the *mean square family size* [24] – which are related to problem hardness – we observe an easy-hard-easy transition in problem hardness as the problems become more diluted, which we associate to the clusterization and connectivity of the underlying Erdős-Rényi graphs [25–28]. After studying this behaviour, we compare the efficiency of SA and PA to find the ground state of this type of problem. These results show that PA has a considerable efficiency advantage over SA for the problem instances generated with a connectivity value around the hardness peak, which vanishes as the connectivity moves away from this value. This is consistent with a physical picture in which PA is advantageous in hard combinatorial optimization problems with intermediate connectivities, where individual samples are likely to get stuck in local minima. Moreover, we expand this study by considering a version of PA that employs an adaptive temperature schedule [24, 29] and demonstrate that this schedule offers a further efficiency improvement as compared to a linear inverse temperature schedule while also being more robust against final temperature miscalibrations.

This work is organized as follows: In Section II we introduce the diluted Sherrington-Kirkpatrick Ising model, which will be the focus of our study. We will also provide a brief explanation of the simulated annealing and population annealing algorithms, and introduce the quantities that we will use to characterize the problem hardness and the relative efficiency between these algorithms. In Section III we investigate the problem hardness by using population annealing simulations and study an easy-hard-easy transition as a function of the density of interactions between spins. We continue by exploring how this problem hardness transition affects the relative efficiency between simulated annealing and population annealing in Section IV, while also benchmarking the efficiency of the adaptive temperature schedule offered by population annealing. Finally, in Section V we present our conclusion to this study.

II. MODEL AND METHODS

A. Diluted SK Model

The Sherrington-Kirkpartrick (SK) [30] Ising spin-glass Hamiltonian is defined as:

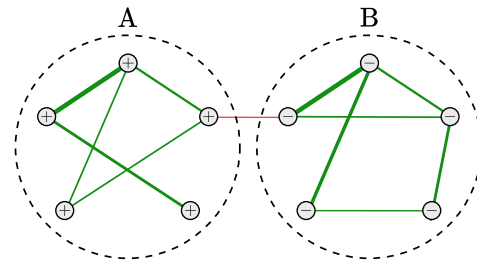$$\mathcal{H} = -\frac{1}{2}\sum_{i,j}^{N} J_{ij}s_i s_j, \tag{1}$$

FIG. 1. Example of a problematic spin configuration for finding the minimum energy configuration using single-spin flip algorithms. For this case, we considered all $J_{ij} \leq 0$, with bigger widths representing more negative values of J_{ij}, and the colors indicate whether the interaction contributes with negative energy (green) or not (red). While clusters A and B are in a local minimum energy configuration, one of these clusters should flip all of its spins to reach the global minimum. However, if the temperature is low, it is unlikely to achieve this by performing single-spin flips.

where $s_i = \pm 1$ represents the value of the i-th spin, of a system of N spins. The matrix J is a symmetric matrix where the entries J_{ij} are sampled from a Gaussian distribution with mean zero and variance of $1/N$. In this work, we study a variation of this model, namely the diluted SK model [22]. This model is similar to the SK model but with the particularity of setting random bonds equal to zero (both J_{ij} and its symmetric J_{ji}) with a probability $1 - p$. To ensure a similar behaviour for different values of p, we set the variance of the entries J_{ij} to $1/Np$, so that the ground state energy is similar for each value of p considered.

The minimization of models such as this one can be problematic when using local search algorithms, like the ones considered in this work which depend on single-spin flip updates. This is due to the appearance of local minima that are separated from the global minimum by high energy barriers [31, 32]. An example of this behaviour is shown in Fig. 1, in which the appearance of weakly interacting clusters can considerably complicate the combinatorial optimization process. In this work, we argue that population annealing, thanks to its resampling step, can help alleviate this type of complication. Therefore, considering the diluted SK model will allow us to study and compare the performance of the simulated annealing and population annealing algorithms, which we introduce in the following, as a function of the connectivity of the problem instances.

B. Simulated Annealing

Simulated Annealing (SA) is a Monte Carlo algorithm that starts with a set of R *replicas* $\mathbf{s}^{(r)}$, $r = 1,...,R$. In our case, these replicas are spin configurations, which have an energy associated with a given Hamiltonian such as the one introduced in Eq. (1). When the spin values

of these replicas are initialized randomly, they can be considered as samples from a Boltzmann distribution at a temperature $T_0 \to \infty$ or inverse temperature $\beta_0 = 1/T_0 \to 0$. Given a replica $\mathbf{s}$ with energy E, it is possible to propose a single-spin flip change that results in a new configuration $\mathbf{s}'$ with energy E'. Using the Metropolis-Hastings rule [15]:

$$P_{\text{accept}}(\mathbf{s}'|\mathbf{s}) = \begin{cases} 1 & \text{if} \quad E' \leq E \\ e^{-\beta_1(E'-E)} & \text{if} \quad E' > E, \end{cases} \quad (2)$$

it is possible to accept or reject changes of this type so that, after proposing enough changes, the initial replicas obtained from a thermal distribution at inverse temperature β_0 are transformed into approximate samples corresponding to a thermal distribution at $\beta_1 > \beta_0$. In our case, the single-spin flips are proposed by performing a total of N_S ordered sweeps over all the spins. The replicas obtained, that approximate samples obtained at inverse temperature β_1, can then be used to obtain samples at a higher value of β. This defines an iterative process that anneals the replicas to increasing inverse temperature values β_t, with $t = 1, ..., N_T$, until reaching a target final temperature. These steps constitute the SA algorithm.

In SA, the R replicas are independent of each other. Thus, the probability of successfully finding the ground state using R replicas, $g(R)$, can be obtained from the probability of finding it with a single copy, $g(1)$, as:

$$g(R) = 1 - [1 - g(1)]^R. \quad (3)$$

Using this expression one can estimate the so-called Time-To-Solution (TTS), which is the number of replicas needed to reach a specific success rate (we will consider 99%). The TTS is then defined as:

$$\text{TTS}_{0.99} = t_{SF} N_S N_T N \frac{\log(1 - 0.99)}{\log(1 - g(1))}, \quad (4)$$

where t_{SF} is the time required to perform a sweep. In the following, we simply set $t_{SF} = 1$ and define the TTS as the number of computational steps.

C. Population Annealing

Population Annealing (PA) [12, 13] is a sequential Monte Carlo algorithm [33] that works similarly to SA but introduces a resampling step when changing the temperature of the system from β_t to β_{t+1}. This resampling is performed between the replicas by associating a probability proportional to the relative Boltzmann weights between each temperature to each replica:

$$\tau_i = \frac{e^{-(\beta_{t+1} - \beta_t)E_i}}{Q(\beta_t, \beta_{t+1})}, \quad (5)$$

with the normalization factor

$$Q(\beta_t, \beta_{t+1}) = \sum_{i=1}^{R} e^{-(\beta_{t+1} - \beta_t)E_i}. \quad (6)$$

There are different ways of resampling using these probabilities. In this work, we implemented the so-called *systematic resampling* approach [34, 35]. This resampling scheme can be visualized by positioning each replica in a line with an associated length equal to its corresponding τ_i value, thus dividing the $[0, 1)$ interval into R segments. The resampling is then implemented by generating a random number $U_0 \in [0, 1/R)$ and selecting R positions within the $[0, 1)$ interval given by the values $U_k = U_0 + k/R$ with $k = 0, ..., R - 1$. Each value of k will be associated with the replica corresponding to the segment where U_k lays, leading to that replica being resampled. This method keeps the number of replicas constant and requires only one randomly generated number for each resampling step. The resampling step helps the algorithm avoid local minima, for which the SA algorithm has no mechanism to escape and would otherwise be trapped, resulting in a reduced number of effective replicas exploring the configuration space. While the resampling process generates copies of configurations, thus introducing correlations, this is alleviated after enough Monte Carlo steps, which decorrelates them through single-spin flip changes. Finally, we note that the time required for the resampling steps is negligible compared to the time needed for the spin-flip part of the algorithm, making the efficiency comparisons between SA and PA straightforward.

An additional advantage of PA is that one can use the statistical information of the samples at each temperature to implement an adaptive inverse temperature schedule [24, 29]. The adaptive schedule used in this work is obtained by considering a *culling fraction*, ϵ, such that at each resampling step a fraction ϵ of the replicas is removed and substituted by resampling of the other replicas. By fixing this culling fraction, one can find the corresponding change in β for each step. While this can be done by using algorithms such as bisection search, we will use the following simple rule derived from considering that at step t the replicas energies are given by a Gaussian distribution with standard deviation $\sigma_{E,t}$:

$$\Delta \beta_t \approx \frac{\epsilon \sqrt{2\pi}}{\sigma_{E,t}}. \quad (7)$$

We note that recent progress has been made in the development of more advanced adaptive schedules, which can be found in Ref. [36]. In this work, we will consider a linear inverse temperature schedule when not considering the adaptive one.

Finally, while it is possible to study the problem hardness by using SA to find the TTS, this approach becomes computationally expensive since it first requires finding the ground state of each problem, and then using SA

with enough replicas R such as to obtain a good success probability estimate. Moreover, this process should be performed for different values of the hyperparameters of SA to obtain an optimized value of the success probability. This becomes more inefficient as the size of the problems increases. Instead, one can use the PA algorithm to estimate and study two similar quantities, namely the *mean square family size* [24], ρ_t, and the *entropic family size* [23], ρ_s, that can be used as criteria for the correct thermalization of the algorithm, as well as for characterizing the complexity of different problems through the study of the free-energy landscape ruggedness. These quantities can be obtained from a single PA run for each problem instance, and have already been used for studying problem hardness since they correlate with other metrics such as the free energy systematic error [24], the time-to-solution [37], and the integrated autocorrelation time in Markov Chain Monte Carlo [23]. Both of these quantities are obtained from the fraction of the final population that descends from the i-th replica of the initial population, n_i. Using this definition, the mean square family size is given by:

$$\rho_t = \lim_{R \to \infty} R \cdot \sum_{i=1}^{R} n_i^2. \tag{8}$$

Similarly, the entropic family size is defined as:

$$\rho_s = \lim_{R \to \infty} R \cdot \exp\left[\sum_{i=1}^{R} n_i \log(n_i)\right]. \tag{9}$$

Large values of ρ_t and ρ_s imply a low survival probability of the initial families and, thus, a more rugged energy landscape. In the following section, we will use these quantities as a measure of the diluted SK model hardness as a function of the parameter p.

III. PROBLEM HARDNESS

We perform simulations applying the PA algorithm to problem instances generated with different sizes N and values of p. We set the inverse temperature to $\beta = 5$ as the final inverse temperature for these simulations. We also set the remaining hyperparameters as $N_S = 10$, $N_T = 100$, and $R = 10^5$. For these values of the hyperparameters and problem instances under consideration, we make sure that $R > 100\rho_s$ and $R > 100\rho_t$ as a condition for thermal equilibration, which also ensures that the values ρ_s and ρ_t are close to their true value.

We show the mean values of $\log(\rho_t)$ and $\log(\rho_s)$ obtained from these simulations as a function of p and for different problem sizes in Fig. 2. Each data point has been obtained by simulating 6000 problem instances and it is normalized to the corresponding mean value of $\log(\rho_t)$ and $\log(\rho_s)$ for that size at the SK limit, i.e., $p = 1$. We can see from these results that the relative values of ρ_t and ρ_s with respect to the SK values increase
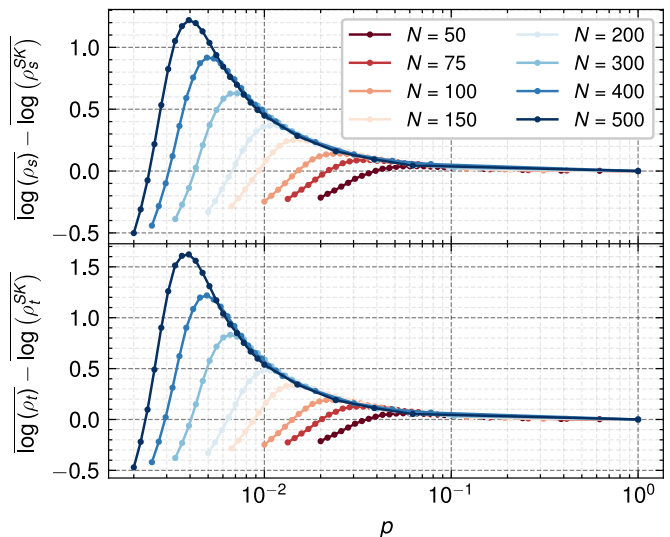

FIG. 2. Mean value of the logarithm of ρ_t and ρ_s as a function of p obtained for different problem sizes and values of p normalized with respect to the corresponding mean value for that size at the SK limit.
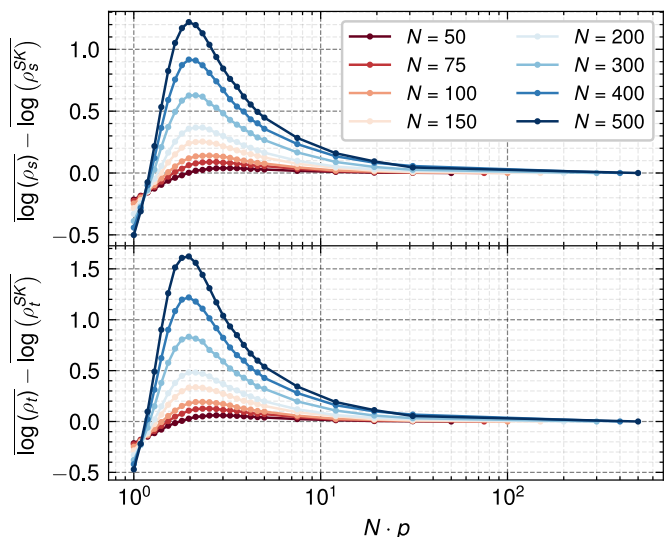

FIG. 3. Mean value of the logarithm of ρ_t and ρ_s as a function of Np obtained for different problem sizes and values of p normalized to the corresponding mean value for each size at the SK limit.

as p decreases similarly for all the problem sizes. However, these values show a peak at different values of p for each problem size. In Fig. 3 we show the same results as a function of Np. From this, we can see that the maximum values of ρ_t and ρ_s approach a value close to $Np \approx 2$ as the problem size increases. We observe from these results that this model presents an easy-hard-easy transition in the problem family hardness as a function of p. Since this behaviour is similar to the one found in Ref. [37], we perform a similar study to better understand this behaviour. We obtain a rough estimate of the asymptotic value of
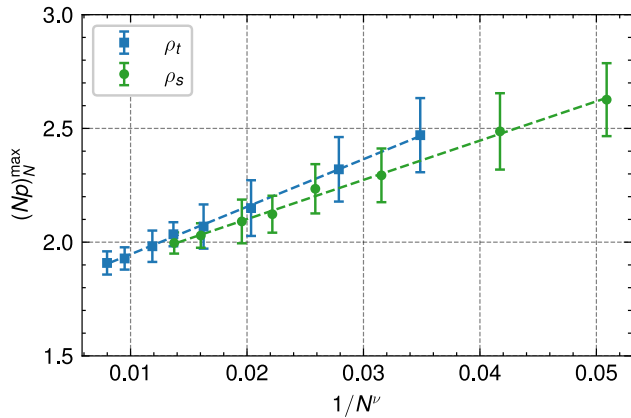
FIG. 4. Results of the fit from Eq. (10) (discontinuous lines) to the values of Np where the maxima of ρ_s and ρ_t occurs for the results in Fig. 3. The error bars are obtained through bootstrap sampling.

FIG. 5. Size of the giant component in Erdős-Rényi graphs for different values of N and Np obtained by calculating the average of 5000 instances for each data point. We also show the asymptotic value for $N \to \infty$.

the hardness peak as $N \to \infty$ from the results shown in Fig. 3. To do this we fit the data points that are close to the peak to a third-order polynomial to estimate the peak positions for that problem size, $(Np)_N^{\max}$, for each size considered. We fit these results to a function of the form:

$$(Np)_N^{\max} = (Np)_{N \to \infty}^{\max} + A/N^{\nu}, \qquad (10)$$

to obtain the estimates of $(Np)_{N \to \infty}^{\max}$, A, and ν. The peak values for each problem size and the corresponding fit are shown in Fig. 4. The values obtained using ρ_s are $(Np)_{N \to \infty, s}^{\max} = 1.76 \pm 0.07$, $A_s = 17.3 \pm 7.0$, and $\nu_s = 0.69 \pm 0.11$ and using ρ_t are $(Np)_{N \to \infty, t}^{\max} = 1.74 \pm 0.05$, $A_t = 20.9 \pm 7.8$, and $\nu_t = 0.78 \pm 0.09$. While these estimated values could be improved by performing more simulations and increasing the size of the problem instances considered, they are enough to get a rough estimation of the asymptotic value of the problem hardness peak.

To understand this easy-hard-easy transition of the diluted SK model, we can consider the properties of the underlying Erdős-Rényi graphs. It is known that, for these graphs, there is a transition that causes the biggest cluster of the graph (also called the *giant component*) to be of size $O(N)$ for values $Np > 1$. The average size of the giant component for different values of N and Np obtained from the simulation of 5000 instances are shown in Fig. 5. Moreover, we also show the asymptotic value that is expected as $N \to \infty$ [27, 28]. Therefore, we can expect two effects as a consequence of increasing the value of Np: First, smaller independent clusters start to connect, resulting in bigger clusters. This is important since one would expect that a problem instance composed of a set of small clusters would be easier to solve than the case in which all these spins are interacting, forming a giant cluster. Secondly, these clusters will show higher interconnectivity between their spins as Np increases. Consequently, there will be fewer cases such as the one explained in Fig. 1, which are expected to
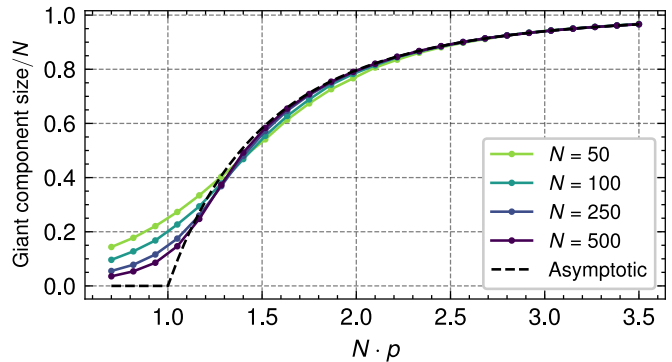
increase the hardness of a problem instance. Therefore, higher connectivity can be expected to decrease the problem hardness. It is at intermediate connectivities that we expect weakly coupled clusters leading to the situation in Fig. 1 and harder problems.

To test these claims, we simulate the effects of the clusterization and the connectivity of each cluster on problem hardness. We consider problem instances with a total of $N = 300$ spins for which we generate spin clusters of the same size S but disconnected from each other. We also consider different connectivities by considering that each cluster is a regular graph of degree D, meaning that each spin is connected to another D spins of the same cluster. The weights of each interaction are then generated in the same way as explained for the diluted SK model. In the following, we only show results for ρ_t, since both ρ_t and ρ_s yield similar results. The results are shown in Fig. 6, where we obtain the values of $\log(\rho_t)$ for each instance and average over 1000 instances for each set of parameters. In Fig. 6 (a) we study the behaviour of ρ_t as the cluster sizes increase. We observe the expected behaviour where, independent of the degree (or connectivity) of the clusters, the hardness of the problem instances increases as the smaller clusters are combined into a set of bigger clusters. This mechanism explains the easy-hard transition found at the left of the hardness peak in Fig. 3, where the values of Np are low resulting in small independent clusters. Similarly, in Fig. 6 (b), we study how the connectivity of each cluster affects the problem hardness for different cluster sizes, including the case where all the spins are part of the same cluster. From this, we observe the same behaviour for all of these cases, where a peak of hardness appears for $D = 3$, but then the hardness drops considerably as the connectivity increases. This explains the hard-easy transition that appears at the right of the hardness peak in Fig. 3. Taking both effects into consideration explains the easy-hard-easy behaviour found in Fig. 3 for the diluted SK model.

After studying the easy-hard-easy transition of the diluted SK model, we now move on to study the distribu-
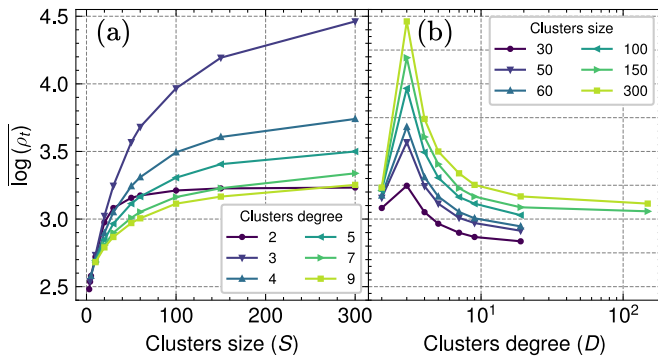
FIG. 6. Study of the problem hardness of clusterized regular graphs for problems of size $N = 300$. (a) Behaviour of ρ_t as the cluster sizes increase for different cluster degrees The result of moving from small independent clusters to a big cluster is an increase in problem hardness. (b) Behaviour of ρ_t as the cluster degree increases for different cluster sizes. As the connectivity of the clusters increases, the problem hardness is considerably reduced.

FIG. 7. Probability distribution of $\log_{10}(\rho_t)$ for different problem sizes and values of p. The continuous lines represent the corresponding fits to the log-inverse Gaussian distribution in Eq. (11).

tions of $\log(\rho_t)$ for problem instances with different values of the problem size and p. The computational hardness of Ising spin glasses has a broad distribution with respect to different disorder realizations [23, 38]. Specifically, ρ_t was found to be approximately distributed as a log-inverse Gaussian distribution when considering 3D Edward-Anderson spin glasses in Ref. [24]. This distribution is given by:

$$P(x; \mu, \lambda, l) = \sqrt{\frac{\lambda}{2\pi(x-l)^3}} \exp\left[\frac{-\lambda(x-\mu-l)^2}{2\mu^2(x-l)}\right],$$

(11)

where $x = \log_{10}(\rho_t)$, $l > 0$ is a parameter that shifts the distribution, and $\lambda > 0$ is a shape parameter. Using the results of the simulations, we approximate the probability distribution of $\log(\rho_t)$ by considering histograms. We fit these histograms to the distribution in Eq. (11) and show the results in Fig. 7. Additionally, the parameters obtained from the fit for $p = 1$ and $Np = 2$ are shown in Table I. From these results, we can confirm that, for a fixed problem size, the problem hardness increases as the value of Np decreases, until reaching a hardness peak. Moreover, the distribution not only moves to higher values of ρ_t but also becomes wider, implying a broader distribution of the problem instance hardness.

	$N = 300$	$N = 400$	$N = 500$
l	(0.93, 1.23)	(0.94, 1.35)	(0.99, 1.45)
μ	(0.78, 0.12)	(1.09, 0.15)	(1.36, 0.17)
λ	(16.3, 0.13)	(27.0, 0.17)	(38.7, 0.23)

TABLE I. Parameters obtained from the fits to Eq. (11) and shown in Fig. 7 for different sizes and for $p = 1$ (left values) and $Np = 2$ (right values).
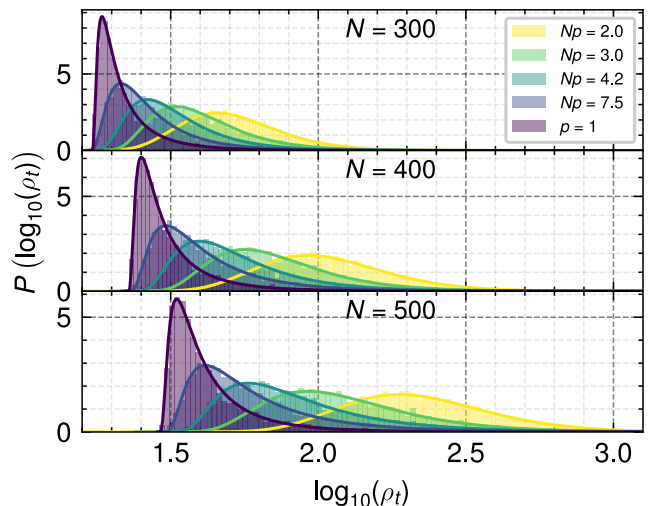
IV. COMPARISON OF THE COMBINATORIAL OPTIMIZATION EFFICIENCY

A. Comparison between SA and PA

We compare the efficiency in finding ground states for both the SA and PA algorithms. To do this, we consider problems with fixed size $N = 200$ for different values of p. We find the ground state for each problem instance by performing PA with $R = 10^5$, $N_T = 100$, $N_S = 20$, and target inverse temperature $\beta_f = 5$. Similarly to the previous section, we require a large number of independent families at the final temperature to be confident about the ground state found by ensuring that the values of ρ_t and ρ_s found satisfy $R \geq 100\rho_t$ and $R \geq 100\rho_s$. Of course, population annealing is a heuristic algorithm and it is not guaranteed that the states that we find are the corresponding ground states. However, in the following study, we have checked that neither the simulation annealing nor the population annealing that we used to benchmark the algorithms managed to find a configuration with a lower energy. Therefore, we will use the energies of these configurations as target energies for the combinatorial optimizations.

Having found these minimum energy configurations for each problem instance, we optimize the parameters of SA to achieve a fair comparison between the two algorithms. We do this by fixing the number of temperature steps N_T and finding the mean TTS value as a function of N_S. Small values of N_S do not guarantee the correct convergence of the Monte Carlo algorithm to a Boltzmann distribution, while too large values lead to an unnecessary long TTS. Each TTS value is found by calculating the value $g(1)$ for each problem and then using Eq. (3)
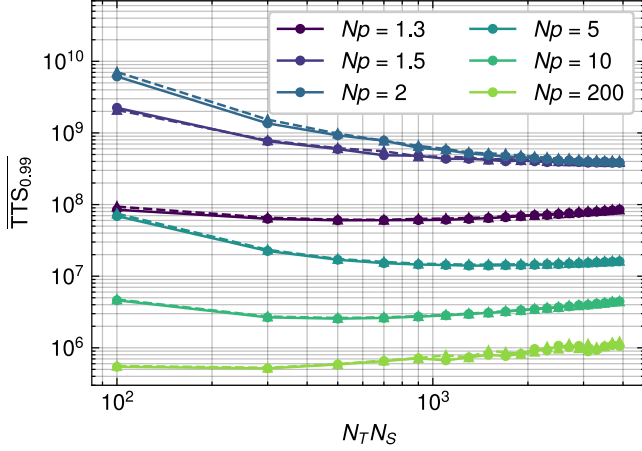
FIG. 8. Mean value of the TTS obtained over 10^3 problem instances of size $N = 200$. Two different values of N_T have been simulated: $N_T = 50$ (triangles with discontinuous lines), and $N_T = 100$ (circles with continuous lines). Both values of N_T result in similar efficiencies, which depend on $N_T N_S$.

FIG. 9. Probability of finding the ground state, P_{success}, averaged over 10^3 problem instances of size $N = 200$ for increasing computational resources for PA (with different values of N_S) and SA with optimized hyperparameters. PA shows a considerable advantage as the value Np decreases.

FIG. 10. Approximation ratio, α, averaged over 10^3 problem instances of size $N = 200$ for increasing computational resources for PA (with different values of N_S) and SA with optimized hyperparameters. As for the probability of success, PA shows a considerable advantage as the value Np decreases.

to extrapolate and calculate the mean TTS. The results are shown in Fig. 8. We do this for $N_T = 50, 100$ and observe a similar behaviour for both cases. In the following, we will use $N_T = 100$ for all the simulations of SA and PA. We observe a considerable increase in the TTS as the problems move from the SK cases to the most diluted ones. We note that optimizing SA for sizes higher than $N = 200$ would require a considerable amount of resources for values of Np close to the hardness peak.

Using these results we obtain the optimal hyperparameters for the SA algorithm for different values of Np. Then, we find the probability of success of SA as a function of the total computational work $W = RN_T N_S$. We also calculate the success probability of PA for $N_S = 1, 5, 10$. Since the replicas are not independent for the PA case, we cannot use Eq. (3). Instead, we perform simulations of PA for increasing values of R several times to obtain estimates of the probability of success. The results of these simulations are shown in Fig. 9. As we can see, the behaviour of the relative efficiency between SA and PA depends considerably on the value of Np. For the $p = 1$ cases, PA seems to behave worse than SA, but this is a consequence of using a higher value of N_S than required. This effect is reduced when considering $N_S = 1$, for which SA and PA behave similarly. This efficiency might be further improved but, in our implementation, we do not consider fewer spin-flips than a sweep per temperature step. More interestingly, PA shows an increasing improvement over SA as the value of Np decreases. For the value $Np = 2$ the PA algorithm shows a clear efficiency improvement compared to SA. Both the TTS and the relative improvement of PA over SA are decreased again for the value $Np = 1.3$, which is away from the hardness peak.
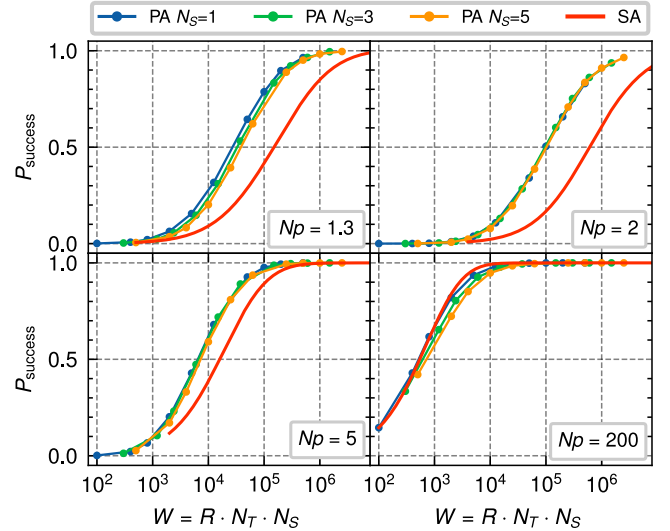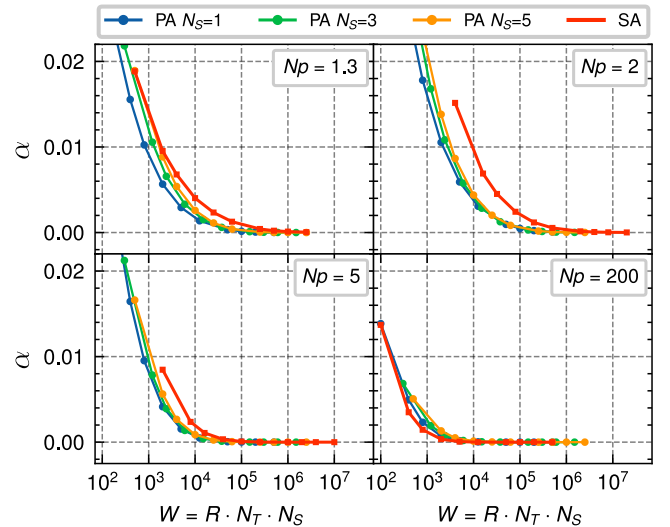
Finally, we perform a similar study considering a

disorder-averaged approximation ratio to the ground state energy, given by:

$$\alpha = 1 - \overline{(E_{\text{min}}/E_0)}, \qquad (12)$$

where E_0 is the minimum energy of a problem instance and E_{min} is the minimum energy found by SA or PA. The results of this study are shown in Fig. 10. From this, we can observe a similar behaviour as for the probability of finding the ground state. For the case with $Np = 2$,

the PA algorithm shows a considerable improvement in accuracy compared to SA, which becomes less noticeable as Np moves away from the hardness peak.

B. Comparison with adaptive temperature schedule

We also compare the relative efficiencies of PA when using a linear inverse temperature schedule and an adaptive one. We use the adaptive schedule described in Sec. II C with a culling fraction of $\epsilon = 0.085$ and increase the inverse temperature until it reaches a target value of β_f. We set a minimum number of replicas, $R_{\min} = 15$, for the adaptive simulations since they require estimating the energy standard deviation at each temperature step. We do this for $\beta_f = 5, 10, 15, 20$. This approach results in a total of $N_T \approx 100$ temperature steps (with some deviation for each problem instance) for each value of Np considered. This resulting value of N_T obtained for each application of the adaptive PA is used for the linear schedule case to ensure that both cases use the same computational resources for each problem instance. The results of these simulations are shown in Fig. 11. From this we observe that the efficiency depends on the value of β_f for the linear case, with $\beta_f = 10$ being the best for the cases close to the hardness peak, while $\beta_f = 5$ is better as the problem instances get easier. This indicates that the linear schedule requires a calibration of the target temperature to achieve optimal performance, with the efficiency being worse for values of β_f below or above this optimal value. As for the adaptive case, we observe that it either reaches a better performance than the linear case for the cases close to the hardness peak, or a similar performance for the easier cases. This is not the case for $\beta_f = 5$, which is apparently a low value. Moreover, the performance of the adaptive schedule seems to be the same as long as β_f is high enough to sample ground state configurations. This makes the adaptive schedule more robust against miscalibrations of the final temperature than the linear schedule.

Finally, we also study the approximation ratios when using both annealing schedules. We follow a similar approach as before, with the results being shown in Fig. 12. From this, we can see similar advantages of the adaptive schedule with respect to the linear one as the ones observed for the probability of finding the ground state. The adaptive schedule is robust in the final temperature chosen while the linear schedule depends on a final temperature that must be calibrated to achieve an optimal efficiency. Furthermore, the adaptive schedule achieves smaller approximation ratios than those obtained from the linear schedules considered. Therefore, from the study of both the probability of finding the ground state and the approximation ratio, we conclude that using an adaptive schedule provides improved efficiency and less dependency on hyperparameters than the linear schedule, without any observed downsides.
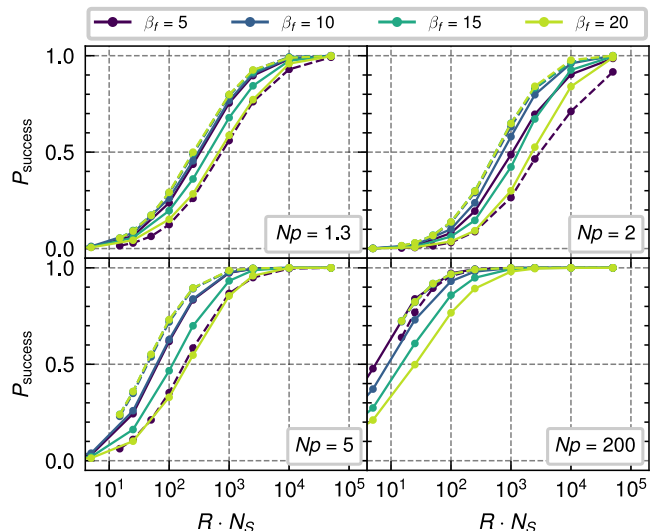

FIG. 11. Probability of finding the ground state, P_{success} using PA with a linear inverse temperature schedule (continuous lines) and an adaptive one (dashed lines), averaged over 10^3 problem instances of size $N = 200$ for increasing computational resources and for different final values of the inverse temperature. Curves representing the PA adaptive case are overlapped for $\beta = 10, 15, 20$.
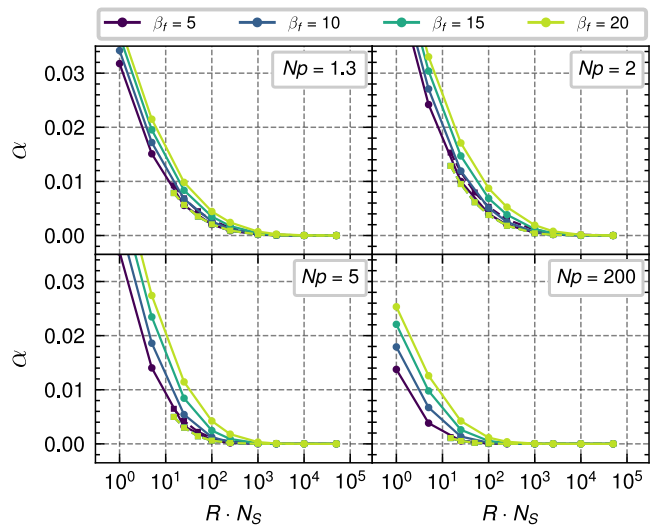

FIG. 12. Approximation ratio, α, obtained using PA with a linear inverse temperature schedule (continuous lines) and an adaptive one (dashed lines), averaged over 10^3 problem instances of size $N = 200$ for increasing computational resources and for different final values of the inverse temperature. Curves representing the PA adaptive case are overlapped for $\beta = 10, 15, 20$.

V. CONCLUSION

In this work, we have studied the problem complexity of the diluted Ising model under the heuristic Population Annealing (PA) algorithm, and we have used this model to benchmark the relative efficiency of PA compared to

Simulated Annealing (SA). Using the mean square family size, ρ_t, and the entropic family size, ρ_s, we managed to quantify the free-energy landscape ruggedness as a function of the problem size, N, and a parameter, p, which controls how much the problems are diluted. From this, we find an easy-hard-easy transition on the hardness of the problems as a function of Np. By studying the effect that the cluster sizes and the connectivity of each cluster have on problem complexity, we conclude that the asymptotic peak of the hardness transition is a consequence of the clusterization and connectivity behaviour of the underlying Erdős-Rényi graphs. Moreover, we also study the probability distribution of ρ_t by fitting the resulting values to a log-inverse Gaussian distribution, as in Ref. [24]. The fitted distributions are in perfect agreement with the data and can be used to estimate the computational resources needed for a correct thermalization of the system using PA. Additionally, these fits show that the increase in hardness as Np approaches the peak is not only related to higher mean values of ρ_t but also to a spreading of the distribution, meaning that the harder problem instances of a family given by a value Np require considerable more computational resources than the corresponding easier instances. As for the Sherrington-Kirkpatrick (SK) limit, $p = 1$, the distribution has both a smaller mean value and variance, meaning that these problems are easier and each instance requires a similar amount of resources to thermalize.

Having found the hardness behaviour of the diluted SK model, we studied the relative efficiency between the SA and PA algorithms to expand the results found in Ref. [16]. To do this, we follow a similar procedure, where we fully calibrate the hyperparameters of SA for a problem size $N = 200$ and different values of p. Using this optimally calibrated SA, we compare it with PA by studying both the probability of success and the approximation ratio as a function of the computational resources. For both of these quantities, we found that the PA algorithm outperformed the SA algorithm for values of Np close to the hardness peak, with this efficiency improvement vanishing as the problems move closer to the SK limit. We assume that this behaviour results from the free-energy landscape becoming less rugged as the problem families reach the SK limit, making the resampling step from PA

less important. However, we note that these results are obtained for a fixed and small value of N that allowed us to study the relative efficiency for values of Np close to the hardness peak, and a higher ruggedness of the free-energy landscape as N increases could result again in an advantage of PA over SA in the SK limit.

Finally, we perform a similar efficiency study comparing two cases of PA: one using a linear inverse temperature schedule and another using an adaptive one. From this study, we find that the efficiency of the linear schedule is considerably dependent on the chosen final inverse temperature. However, the adaptive schedule seems independent of the final temperature as long as it is high enough to sample the ground state configuration, making this type of schedule more robust under miscalibrations of the final inverse temperature. Moreover, the adaptive schedule showed a slight efficiency improvement for problems close to the hardness peak compared to the best final inverse temperature found for PA with a linear schedule.

Our work shows that the PA algorithm is ideally suited for combinatorial optimization problems of varying connectivity. This is relevant for practical applications where PA has the additional advantage of providing us with an adaptive method for hyperparameter selection. Moreover, an additional feature of PA is that problem hardness can be estimated by measures like the entropic family size.

[1] V. Černý, Journal of Optimization Theory and Applications **45**, 41 (1985).
[2] D. S. Johnson, in *International colloquium on automata, languages, and programming* (Springer, 1990) pp. 446–461.
[3] R. Mansini and M. G. Speranza, European Journal of Operational Research **114**, 219 (1999).
[4] Y. Crama and M. Schyns, European Journal of Operational Research **150**, 546 (2003).
[5] Álvaro Rubio-García, S. Fernández-Lorenzo, J. J. García-Ripoll, and D. Porras, Physica A: Statistical Mechanics and its Applications **639**, 129637 (2024).
[6] S. F. Edwards and P. W. Anderson, Journal of Physics F: Metal Physics **5**, 965 (1975).
[7] M. Mézard, G. Parisi, and M. A. Virasoro, *Spin glass theory and beyond: An Introduction to the Replica Method and Its Applications*, Vol. 9 (World Scientific Publishing Company, 1987).
[8] F. Barahona, Journal of Physics A: Mathematical and General **15**, 3241 (1982).
[9] G. Jaumà, J. J. García-Ripoll, and M. Pino, Advanced Quantum Technologies **7**, 2300245 (2024).

[10] S. Kirkpatrick, C. D. Gelatt Jr, and M. P. Vecchi, Science **220**, 671 (1983).

[11] R. H. Swendsen and J.-S. Wang, Physical Review Letters **57**, 2607 (1986).

[12] K. Hukushima and Y. Iba, in *AIP Conference Proceedings*, Vol. 690 (American Institute of Physics, 2003) pp. 200–206.

[13] J. Machta, Physical Review E **82**, 026704 (2010).

[14] Álvaro Rubio-García, J. J. García-Ripoll, and D. Porras, arXiv preprint arXiv:2210.00807 (2022).

[15] C. P. Robert, G. Casella, and G. Casella, *Monte Carlo statistical methods*, Vol. 2 (Springer, 1999).

[16] W. Wang, J. Machta, and H. G. Katzgraber, Physical Review E **92**, 013303 (2015).

[17] R. Albert, H. Jeong, and A.-L. Barabási, Nature **401**, 130 (1999).

[18] M. Faloutsos, P. Faloutsos, and C. Faloutsos, ACM SIG-COMM computer communication review **29**, 251 (1999).

[19] M. E. Newman, D. J. Watts, and S. H. Strogatz, Proceedings of the national academy of sciences **99**, 2566 (2002).

[20] G. Robins, T. Snijders, P. Wang, M. Handcock, and P. Pattison, Social networks **29**, 192 (2007).

[21] M. E. Newman, Physical Review E **66**, 016128 (2002).

[22] S. Boettcher, Physical Review Letters **124**, 177202 (2020).

[23] W. Wang, J. Machta, and H. G. Katzgraber, Physical Review E **92**, 063307 (2015).

[24] C. Amey and J. Machta, Physical Review E **97**, 033301 (2018).

[25] P. Erdős and A. Rényi, Publicationes Mathematicae Debrecen **6**, 18 (1959).

[26] P. Erdős, A. Rényi, *et al.*, Publ. Math. Inst. Hung. Acad. Sci **5**, 17 (1960).

[27] B. Bollobás, *Random Graphs* (Springer, 1998).

[28] A. Frieze and M. Karoński, *Introduction to random graphs* (Cambridge University Press, 2015).

[29] L. Y. Barash, M. Weigel, M. Borovskỳ, W. Janke, and L. N. Shchur, Computer Physics Communications **220**, 341 (2017).

[30] D. Sherrington and S. Kirkpatrick, Physical Review Letters **35**, 1792 (1975).

[31] P. Svenson, Physical Review E **64**, 036122 (2001).

[32] H. G. Katzgraber, in *Journal of Physics: Conference Series*, Vol. 95 (IOP Publishing, 2008) p. 012004.

[33] A. Doucet, N. De Freitas, and N. Gordon, Sequential Monte Carlo methods in practice , 3 (2001).

[34] D. Gessert, W. Janke, and M. Weigel, Physical Review E **108**, 065309 (2023).

[35] F. Martínez-García, F. R. F. Pereira, and P. Parrado-Rodríguez, arXiv preprint arXiv:2405.03776 (2024).

[36] A. Barzegar, F. Hamze, C. Amey, and J. Machta, Physical Review E **109**, 065301 (2024).

[37] D. Perera, F. Hamze, J. Raymond, M. Weigel, and H. G. Katzgraber, Physical Review E **101**, 023316 (2020).

[38] B. Yucesoy, J. Machta, and H. G. Katzgraber, Physical Review E **87**, 012104 (2013).